The tumor-associated EpCAM regulates morphogenetic movements through intracellular signaling

Nadim Maghzal, Emily Vogt, Wolfgang Reintsch, James S. Fraser, and François Fagotto

Department of Biology, McGill University, Montreal, Quebec, Canada H3G 0B1

Epithelial cell adhesion molecule (EpCAM) is best known as a tumor-associated protein highly expressed in carcinomas. The function of this cell surface protein during embryonic development and its potential role in cancer are still poorly understood. We identified EpCAM in a gain-of-function screen for inducers of abnormal tissue mixing during gastrulation. Elevated EpCAM levels in either the ectoderm or the mesoderm confer "invasive" properties to cells in both populations. We found that this phenotype represents an "overstimulation" of an essential activity of EpCAM in controlling cell movements during embryonic development. Surprisingly, this property is independent of the putative adhesive function of EpCAM, and rather relies on a novel signaling function that operates through down-regulation of PKC activity. We show that inhibition of novel PKCs accounts entirely for the invasive phenotype induced by abnormally high levels of EpCAM as well as for its normal function in regulating cell rearrangement during early development.

Introduction

EpCAM has been long known as a tumor-associated antigen highly expressed in a variety of carcinomas (Koprowski et al., 1979). It is used as a marker for aggressive tumors, and has been considered as a potential target for immunotherapy (Osta et al., 2004). In human and mouse, EpCAM is expressed in embryonic epithelia, but the levels usually drop as cells reach terminal differentiation (Trzpis et al., 2007). Enhanced expression of EpCAM is associated with active proliferations of neoplastic or normal tissues (de Boer et al., 1999). The protein can act as a homophilic Ca^{2+}-independent cell–cell adhesion molecule (Litvinov et al., 1994). It is not structurally related to any of the major families of CAMs, but a potential link to the actin cytoskeleton via α-actinin has been documented (Balzar et al., 1998). Thus, it was initially proposed that enhanced proliferation and migration in cells expressing high levels of EpCAM resulted from sequestering α-catenin away from E-cadherin (Litvinov et al., 1997). However, a recent study has shown that EpCAM is required to maintain the integrity and plasticity of the zebrafish developing epidermis where it works in partial redundancy with E-cadherin to promote cell–cell adhesion (Slanchev et al., 2009). Another study indicates that the enhancing effect of EpCAM on proliferation rates of carcinoma may in fact largely rely on a signaling activity of its intracellular domain (Münz et al., 2004; Maetzel et al., 2009). This short segment can be cleaved and is then able to form a complex with FHL2, β-catenin, and Lef-1 that induces gene transcription of oncogenes such as C-myc and cyclins A/E. Thus, the role of EpCAM in cell–cell adhesion and the relative contributions of its potential adhesive and signaling activities in morphogenesis and proliferation remain unclear.

Xenopus gastrulation is an established model to study morphogenetic movements. During this phase of development, the embryo undergoes massive reorganization. Because there is very little cell division and no increase in total cell mass at this stage, the whole process relies purely on rearrangement of preexisting tissues. In particular, the ectoderm thins and expands to eventually cover the whole embryo (epiboly), while the mesoderm moves inside the embryo through involution, and migrates along the inner surface of the ectoderm (blastocoel roof [BCR]).

N. Maghzal and E. Vogt contributed equally to this paper.

Correspondence to François Fagotto: francois.fagotto@mcgill.ca

J.S. Fraser's present address is Dept. of Molecular and Cell Biology, University of California, Berkeley, Berkeley, CA 94720.

Abbreviations used in this paper: BCR, blastocoel roof; Bis1, bisindolylmaleimide I; EpCAM, epithelial cell adhesion molecule; PMA, phorbol-12-myristate-13-acetate.

The Rockefeller University Press $30.00
J. Cell Biol. Vol. 191 No. 3 645–659
www.jcb.org/cgi/doi/10.1083/jcb.201004074

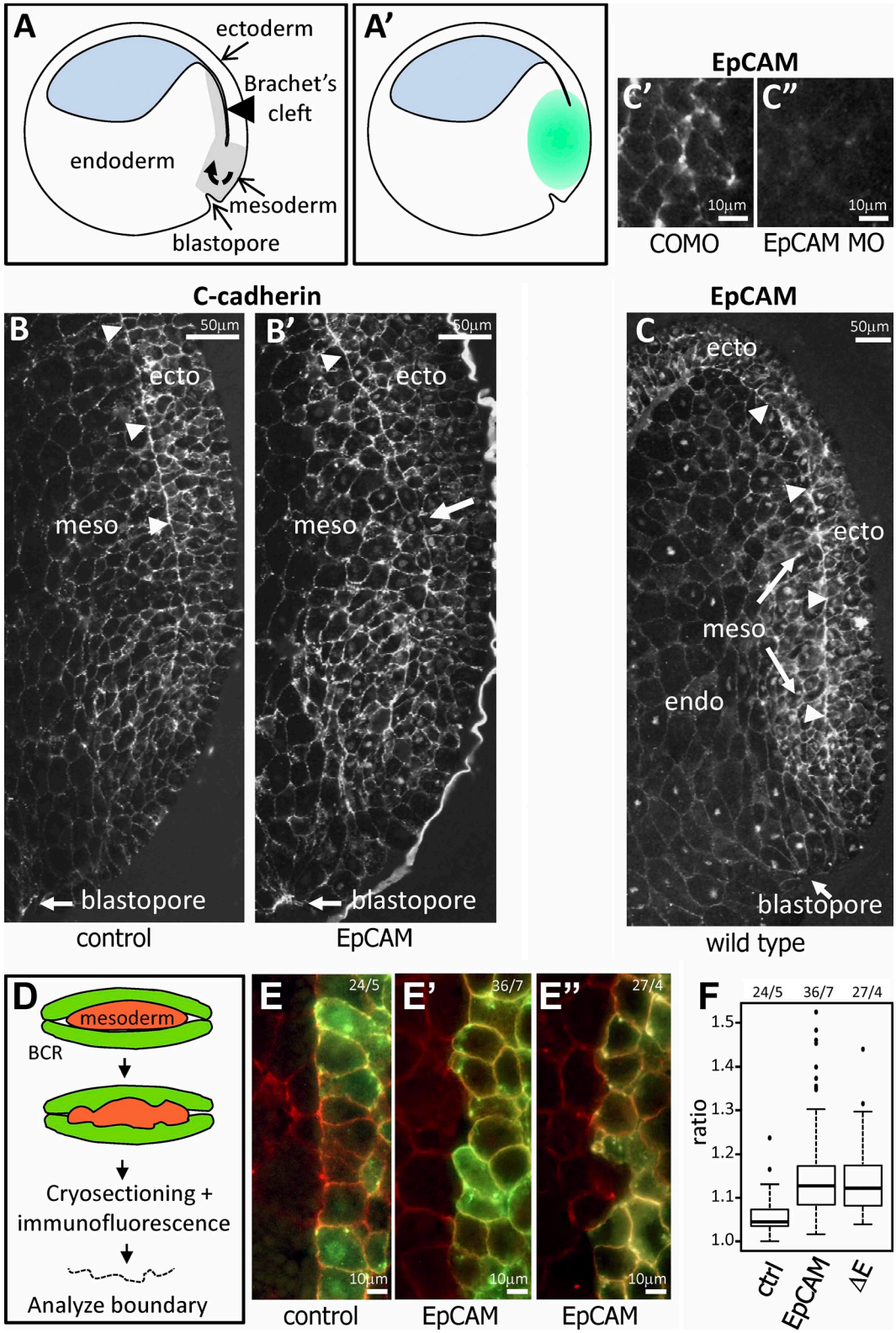

Figure 1. **Identification of EpCAM as inhibitor of the ectoderm–mesoderm boundary.** (A) Diagram of an early *Xenopus* gastrula (stage 10.5). Curved arrow indicates direction of mesoderm involution. (A') Test for disruption of the ectoderm–mesoderm boundary (Brachet's cleft) by dorsal injection of mRNA (green). (B and B') Sagittal views of the dorsal region of embryos injected with control GFP mRNA (B) or EpCAM mRNA (B'). The boundary (arrowheads) is disrupted in the posterior region (arrow) of EpCAM-overexpressing embryos. Cryosections were stained with anti–C-cadherin antibody. Note that exposure has been increased for controls to match the staining intensity of EpCAM-expressing samples. For proper comparison of C-cadherin levels, see Fig. 3. (C) Ubiquitous expression of endogenous EpCAM in all three germ layers, ectoderm (ecto), mesoderm (meso), and endoderm (endo) of the early gastrula. Arrowheads point to Brachet's cleft. (C'–C'') Detail of ectoderm from cryosections of control MO (COMO) and EpCAM MO-injected embryos stained with anti-EpCAM antibody, demonstrating antibody specificity. (D–F) Reconstituted boundaries made of dissected wild-type mesoderm sandwiched between

We are particularly interested in the mechanisms that maintain the mesoderm separated from the overlying BCR, which is essential for proper gastrulation to proceed. This system is also more of interest as it deals with interactions between prototypical forms of epithelial and mesenchymal tissues. The ectoderm–mesoderm boundary can be particularly well studied in *Xenopus*, where it can be reconstituted in an in vitro assay using tissue explants (Winklbauer and Keller, 1996; Wacker et al., 2000). On the mesodermal side, the control of separation seems to depend in part on a still poorly characterized noncanonical Wnt pathway leading to PKC activation (Winklbauer et al., 2001). An interaction between the Wnt receptor Frizzled-7, the protocadherin PAPC, and the ankyrin repeat domain protein 5 xANR5, as well as downstream RhoA and Rho kinase appear to be involved (Hukriede et al., 2003; Medina et al., 2004; Chung et al., 2007). Information is lacking about the mechanisms regulating separation on the ectodermal side.

We have identified the *Xenopus* orthologue of EpCAM in a gain-of-function screen to identify gene products that cause aberrant ectoderm–mesoderm tissue mixing at gastrula stages. We show that the overexpression of EpCAM in either the ectoderm or the mesoderm causes both tissues to mix. More generally, we show that EpCAM levels crucially regulate movements of cells in embryonic tissues. We demonstrate that this effect is not due to an adhesive function of EpCAM, but to a signaling activity involving novel PKC isoforms.

Results

Identification of *Xenopus* EpCAM as a promoter of cell mixing between ectoderm–mesoderm

We identified a *Xenopus* orthologue of human EpCAM in a gain-of-function screen for gene products perturbing the ectoderm–mesoderm boundary, called Brachets' cleft. When EpCAM mRNA was injected in the dorsal region (Fig. 1 A′, green area), the embryos displayed a significant reduction of the posterior part of cleft (Fig. 1, B–B′). BLAST search revealed that *Xenopus laevis* has two closely related EpCAM genes. Their amino acid sequences are highly similar to each other and to EpCAM from other vertebrate species (Fig. S1). All subsequent experiments were performed using constructs based on the EpCAMa clone originally identified in our screen.

To analyze the effect of EpCAM on tissue mixing, we used a well-established in vitro assay (Wacker et al., 2000), where dissected explants are pressed against a blastocoel roof (BCR), which is constituted of ectoderm (Fig. 2 A). Explants of ectodermal origin readily mix in the BCR, whereas wild-type mesoderm explants stay out. Note that compared with the original assay, we introduced an intermediate "fused" category corresponding to a partial loss of separation behavior (blurred boundary, yet explants still bulging out of the BCR). This phenotype is observed at low frequency with wild-type mesoderm.

Consistent with the cleft phenotype observed in whole embryos, we found significant mixing upon EpCAM overexpression. Remarkably, EpCAM caused the same phenotype when expressed either in the BCR or in the mesoderm (Fig. 2, B and C). Simultaneous expression in both tissues did not strengthen the phenotype (unpublished data). The effect appeared dose dependent, peaking around an mRNA dose of 250–300 pg/injection.

We also examined reconstituted boundaries obtained by juxtaposition of dissected BCRs and mesoderm by cryosectioning and immunofluorescence (Fig. 1 D). Compared with control boundaries (Fig. 1 E), the interface between EpCAM-overexpressing BCRs and mesoderm was more irregular (Fig. 1 E′), and cells from one tissue could be found to intrude into the other tissue (Fig. 1 E′′). In a few cases single ectodermal cells were even found isolated in the middle of the mesoderm explants (not depicted), which is never observed for wild-type tissues. Quantitative analysis of "rectilinearity" confirmed that upon EpCAM overexpression the interface departed very significantly from the relative straightness measured in controls (Fig. 1 F).

Endogenous EpCAM is expressed in both ectoderm and mesoderm

EpCAM transcripts are present maternally and throughout development (unpublished data). We determined EpCAM protein localization by immunofluorescence on cryosections using an antibody raised against its cytoplasmic tail. Unlike the epithelial-specific expression reported in mammalian embryos and adult tissues, *Xenopus* EpCAM is ubiquitously expressed in the gastrulating embryo (Fig. 1 C). Some regional differences were observed, levels being highest in the ectoderm and lowest in the endoderm, but such differences may mostly reflect the default distribution of maternally inherited components, as a graded distribution is also observed for C-cadherin (Fig. 1 B) and for a variety of other proteins (unpublished data). Interestingly, EpCAM was slightly but reproducibly enriched at the cleft (arrowheads). EpCAM staining was strongly decreased in embryos injected with morpholino antisense nucleotides targeting both EpCAM alleles (EpCAM MO), demonstrating the specificity of the antibody (Fig. 1, C′–C′′).

EpCAM-induced mixing is mediated by its cytoplasmic domain

To determine which EpCAM domains were required for induction of mixing, deletion mutants of EpCAM lacking the extracellular domain (ΔE) or the cytoplasmic tail (ΔC) were tested,

two injected BCRs, analyzed by cryosectioning and immunofluorescence. (D) Diagram of the assay. (E–E′′) Examples of a control boundary (E) and of the irregular interfaces observed between wild-type mesoderm and EpCAM-overexpressing BCR (E′, E′′). Membrane GFP was coexpressed as tracer. Cell contours were visualized using an anti–β-catenin (red) and injected ectodermal cells with anti-GFP ab (green). (F) Quantification of boundary straightness (see Materials and methods), represented in box plots (50% of the data are within the box, the median is represented by a horizontal line, the whiskers indicate the maximum and minimum value, without outliers, and the single dots the outliers). 1 corresponds to a perfectly rectilinear boundary, high values to convoluted lines, reflecting tissue mixing. EpCAM and its ΔE mutant caused significant mixing compared with controls ($P < 0.001$, Tukey-HSD test). Numbers on top represent number of fields/number of sandwiches (from three independent experiments).

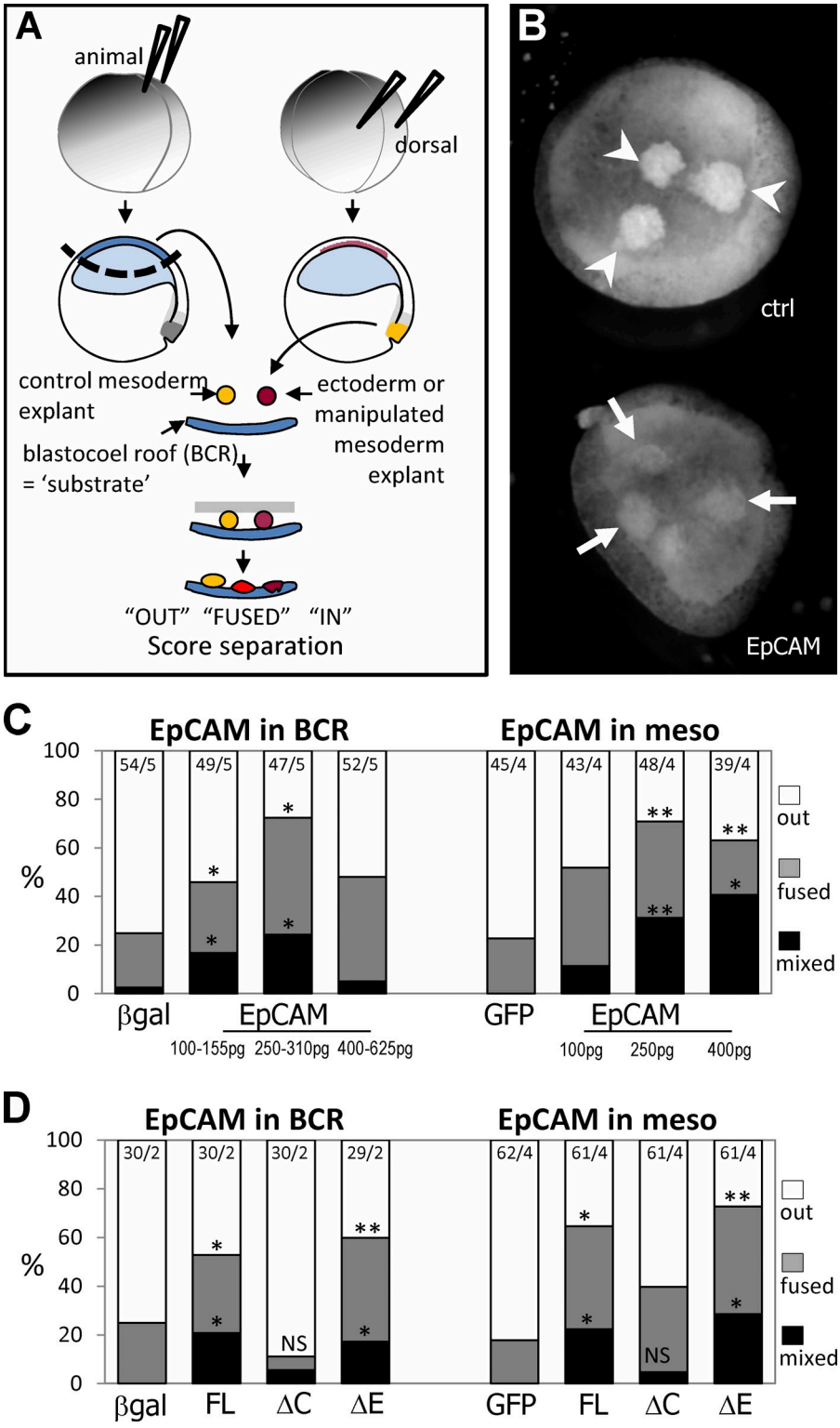

Figure 2. **EpCAM induces ectoderm–mesoderm tissue mixing.** (A) Diagram of the in vitro tissue separation assay. mRNA is injected animally at the 2-cell stage for BCR expression and dorsally at the 4-cell stage for mesoderm expression. At stage 10+, explants and BCRs are dissected and combined, and the degree of separation is scored as "out" (complete separation), "fused," or "mixed." (B) Roof assay of control GFP-expressing and EpCAM-overexpressing mesoderm on wild-type BCRs. The three EpCAM-overexpressing mesoderms, distinguishable thanks to their lighter color, have mixed with the BCR, whereas control explants have remained out. (C) Quantification of tissue mixing induced by EpCAM in the BCRs or in the mesoderm. mRNA amounts/injection are indicated. β-Gal and membrane GFP mRNAs were used as controls. (D) The extracellular domain of EpCAM is dispensable for induction of tissue mixing. Quantification of tissue mixing upon expression in the BCR (C) or the mesoderm (D) of full-length EpCAM (FL), or mutant constructs lacking the cytoplasmic tail (ΔC) or the extracellular domain (ΔE). In both tissues, the cytoplasmic tail is required for activity, but the extracellular domain is dispensable. Numbers on top indicate total number of explants/number of experiments. * and **, $P < 0.05$ and $P < 0.01$, respectively, compared with controls (Student's *t* test).

both in the BCR and in the mesoderm (Fig. 2 D). ΔE, but not ΔC, induced mixing as efficiently as wild-type EpCAM, in both tissues. The mixing activity of the ΔE mutant was also observed on sections of reconstituted boundaries (Fig. 1 F). These surprising results showed that the homophilic binding and adhesive function of EpCAM were dispensable for the mixing phenotype and suggested that signal transduction might be involved.

We further dissected the sequence requirements for this activity using a series of ΔE mutants (Fig. S2). We determined that a short basic segment (RRKKGKYR) is sufficient for EpCAM function, and mutations within this cluster point to a requirement for specific residues (Fig. S2). The same segment of human EpCAM has been reported to bind α-actinin (Balzar et al., 1998). However, we failed to reproduce this interaction with the cytoplasmic tail of *Xenopus* EpCAM (unpublished data).

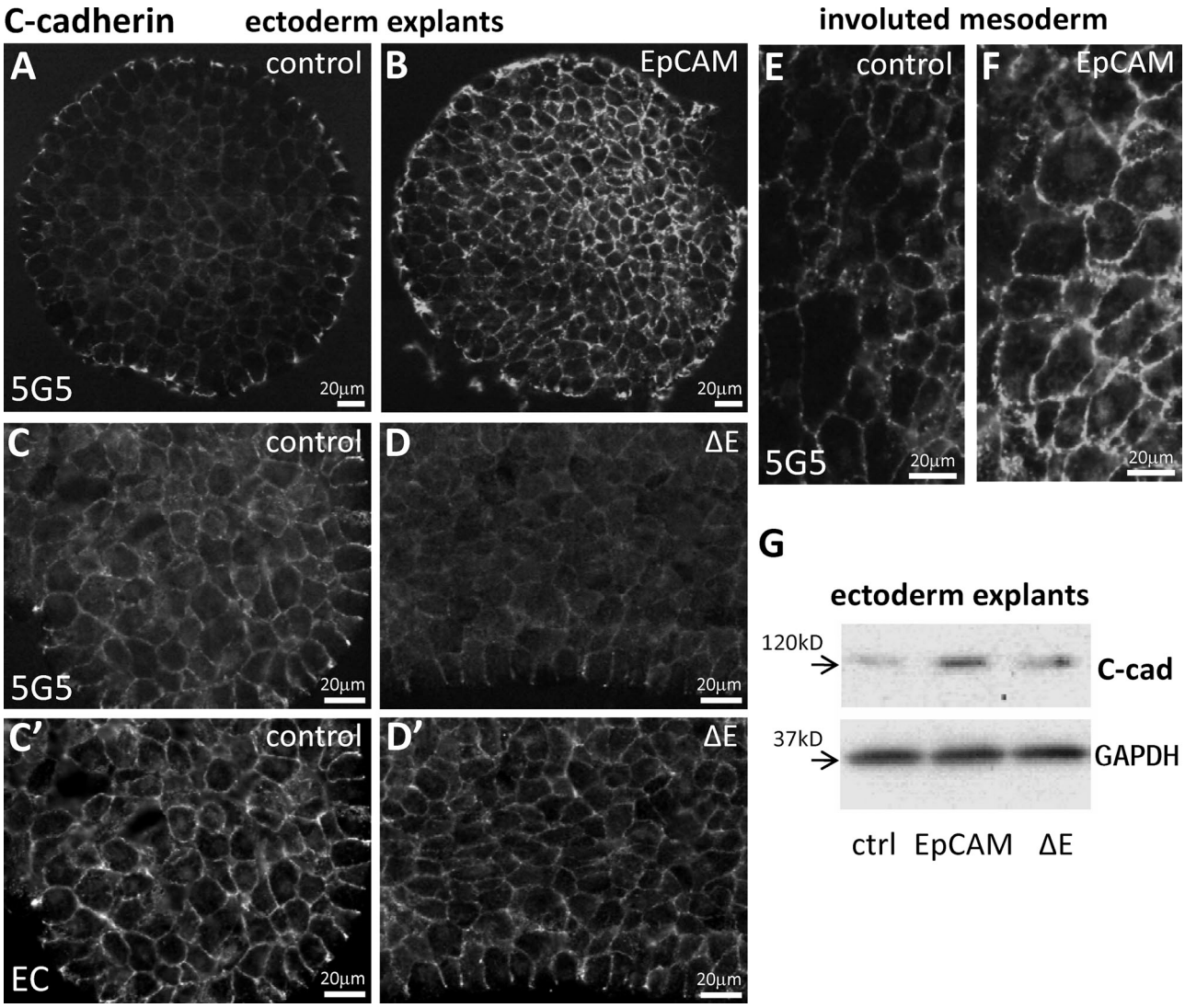

Figure 3. **C-Cadherin levels are increased by wild-type EpCAM but not by ΔE EpCAM.** (A–F) Sections of control membrane GFP, wild-type EpCAM, or ΔE EpCAM-expressing tissues (200 pg mRNA/injection) stained for C-cadherin. (C and D) Double staining using mouse monoclonal 5G5 (C and D) or rabbit polyclonal CE antibodies (C′ and D′). Note that exposure has been increased in C and D compared with A and B. (E) Western Blot comparing C-cadherin levels in control GFP- and EpCAM or ΔE-expressing ectoderm explants.

Tissue mixing does not correlate with cadherin stabilization

In zebrafish embryos mutant for EpCAM, E-cadherin expression in ectodermal cells is decreased (Slanchev et al., 2009). We similarly found that EpCAM-overexpressing cells had strongly increased levels of C-cadherin, the major cadherin expressed in *Xenopus* gastrulating embryos (Fig. 3). Importantly, this increase was observed in both ectoderm (Fig. 3, A, B, and G) and mesoderm (Fig. 3, E and F). ΔE expression had a different effect: although total levels were not affected (Fig. 3 G), two different anti-cadherin antibodies showed significant reduction of the cell membrane staining (Fig. 3, D and D′). We have not been able to determine the cause of this lower signal, possibly due to more diffused membrane distribution, increased internalization, or decreased antibody accessibility. Note that the decreased cadherin staining is consistent with the fact that, unlike wild type, ΔE caused cell dissociation at later stages (unpublished data). Despite these differences, wild-type and ΔE EpCAM could both induce mixing, when expressed in either tissue, suggesting that the effect on tissue separation was uncoupled from the effect on cadherin levels. This is inconsistent with a cell-sorting mechanism based on classical differential adhesion.

EpCAM stimulates "intratissular" cell movements

We wondered whether EpCAM might regulate a different property common to both ectodermal and mesodermal cells, perhaps the ability of cells to move among other cells. To address this question, we looked at "intratissular" movements (Fig. 4 A) in a "sandwich" prepared by pressing against each other two BCRs, one of which was manipulated, the other one wild type. After a 2-h incubation, the sandwich was fixed and the position of the cells analyzed on cryosections. The rationale was that if cells move relative to their neighbors, the initial straight interface created by the apposition of the two BCRs would become progressively more irregular, and a mosaic pattern could eventually appear.

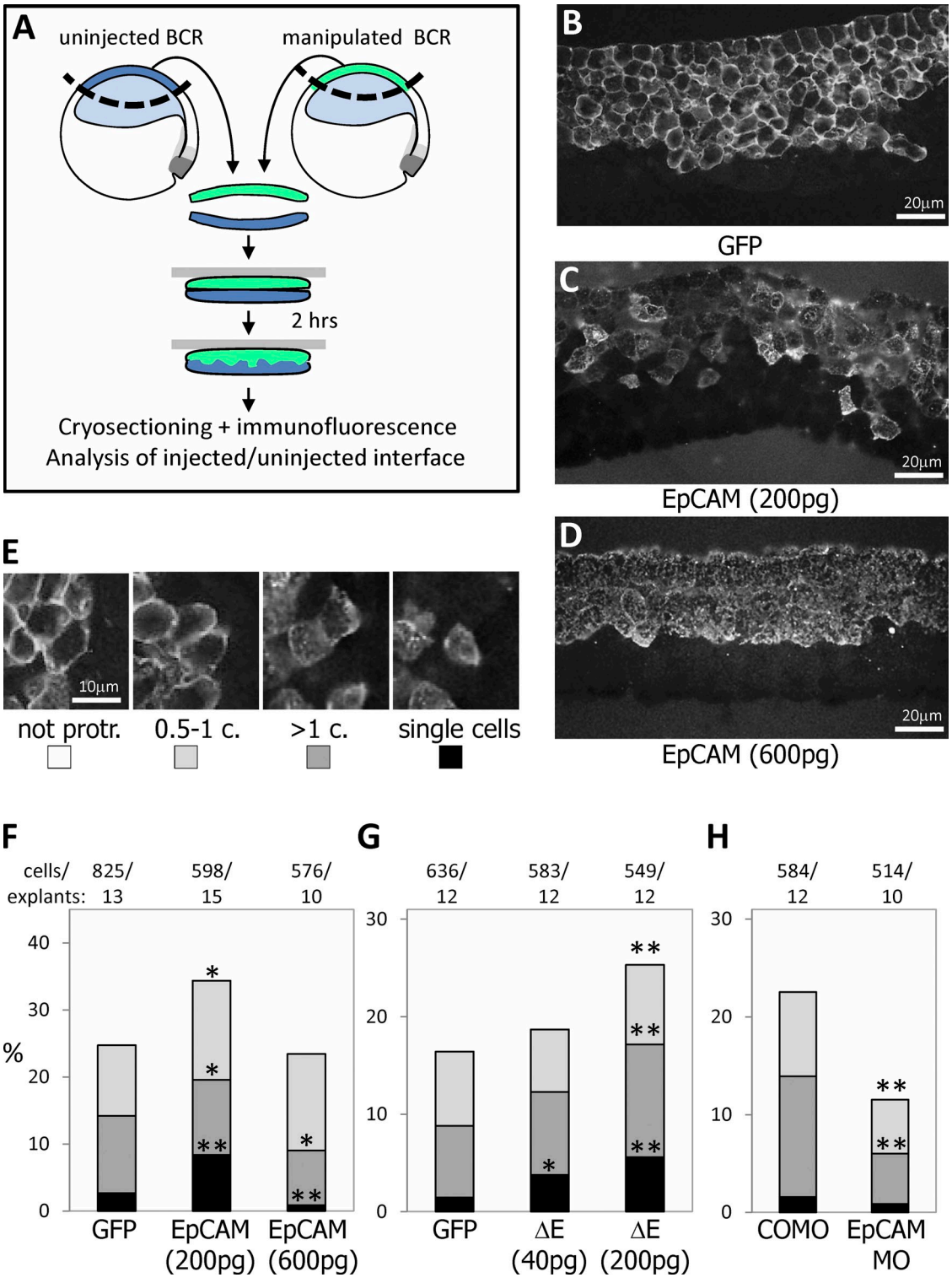

Figure 4. **EpCAM stimulates cell migration within the ectodermal tissue.** (A) Schematic representation of a migration assay in ectoderm explants. Sandwiches were produced by combining wild-type uninjected BCRs with BCRs injected with various mRNAs coding for membrane GFP, EpCAM-MT (see Fig. S2) or ΔE, or with EpCAM MO or COMO (coinjected with membrane GFP mRNA to trace injected cells). The degree of mixing was scored by determining the relative position of individual injected cells, immunostained for GFP or Myc, at the interface with wild-type cells. (B–D) Examples of sandwiches with BCRs expressing control membrane GFP, and low and high levels of EpCAM. (E) Illustration of the four categories used to score cell migration: cells protruding less than 1/2 cell diameter relative to their neighbors (nonprotr.), cells protruding between 1/2 and 1 diameter (0.5–1), or more than one cell diameter (>1), and cells entirely surrounded by wild-type cells (single cells). (F–H) Quantification. Cells moderately overexpressing EpCAM tended to migrate significantly more, whereas cells with high EpCAM levels remained more compacted. Cells expressing ΔE also showed increased migration, for both mRNA doses tested. On the contrary, cells depleted of EpCAM (EpCAM MO) remained significantly more compact. Numbers on top indicate total number of explants/number of experiments. * and **, $P < 0.05$ and $P < 0.01$, respectively, compared with controls (Student's *t* test; see Materials and methods).

The position of the manipulated cells at this interface was scored using a scale of increasing mobility, from "nonprotruding" (i.e., straight boundary) to "single cells" (i.e., mosaic distribution; Fig. 4 E). Because EpCAM-induced ectoderm–mesoderm mixing had shown to peak around 250 pg/injection, we tested two concentrations, 200 and 600 pg. The patterns observed were striking (Fig. 4, B–D): compared with GFP controls, many more cells mildly overexpressing EpCAM had moved away and were found as single cells in the wild-type half of the sandwich (Fig. 4 E). Single and protruding cells added together were also significantly more numerous. The highest amount of EpCAM, however, had the opposite effect: the boundary remained straighter than in the controls (Fig. 4, D and E). Thus, EpCAM displays a bimodal activity, stimulating cell movements at moderate levels, but decreasing it at higher levels, fully consistent with the results of the mesoderm-BCR assays.

We found that the ΔE mutant could also stimulate migratory activity (Fig. 4 E) when expressed at levels that induced efficient tissue mixing (40 pg, Fig. 2). However, stronger expression did not lead to compaction as observed with wild-type EpCAM: on the contrary, migration increased at 200 pg mRNA (Fig. 4 E). Higher levels caused the disaggregation of ectoderm cells (not depicted).

Depletion of endogenous EpCAM interferes with ectoderm cell rearrangement

EpCAM depletion did not cause obvious defects in ectoderm–mesoderm boundary formation (unpublished data), but the BCR of the early gastrula was significantly thicker than normal (Fig. 5, A–D and H), indicating that epiboly, a process that involves radial intercalation and leads to expansion and thinning of the tissue (Keller, 1980), was impaired. The phenotype was fully rescued by coinjection of mRNA coding for full-length EpCAM but lacking 5′ UTR recognized by the morpholinos (Fig. 5, E and H). In zebrafish, a similar phenotype has been reported, and has been mostly discussed based on the presumed adhesive function of EpCAM (Slanchev et al., 2009). Here, we directly addressed this issue by testing the ability of ΔE to rescue epiboly in the EpCAM MO–injected embryos. ΔE could fully rescue a normal BCR (Fig. 5, F and H), demonstrating that the extracellular domain, and thus homophilic binding, are dispensable for this function.

EpCAM depletion also inhibited cell movement in the BCR sandwich assay: EpCAM-depleted BCRs remained significantly more compact, maintaining a sharp boundary with the apposing wild-type BCR (Fig. 4 H).

EpCAM-induced tissue mixing is independent of β-catenin signaling

Because the EpCAM cytoplasmic tail can act as a signal transducer together with β-catenin and Lef1/TCF (Maetzel et al., 2009), we tested the ability of a dominant-negative xTCF3 construct (dnTCF) to interfere with EpCAM-induced mixing. The efficiency of dnTCF to block β-catenin/TCF-Lef signaling was verified using the well-established axis-duplication assay (Molenaar et al., 1996; Fagotto et al., 1997; Zeng et al., 1997). At doses that completely blocked β-catenin–induced axis duplication (Fig. 6 B), dnTCF had no effect on EpCAM-induced tissue mixing (Fig. 6 A), demonstrating that β-catenin/TCF signaling is not involved in this phenotype.

EpCAM operates via down-regulation of PKC activity

PKC signaling in the mesoderm has been implicated at the ectoderm–mesoderm boundary downstream of frizzled 7 (Winklbauer et al., 2001). Specifically, frizzled 7 depletion in the mesoderm caused tissue mixing, which could be rescued by overexpression of PKC-α (and thus presumably PKC overactivation). We therefore sought to determine whether EpCAM-induced mixing may be related to PKC. We first attempted to rescue separation by directly activating PKC using the phorbol ester phorbol-12-myristate-13-acetate (PMA). A short pretreatment of EpCAM-expressing mesoderm explants with a low concentration of PMA efficiently rescued separation (Fig. 6 C). Similarly, PMA treatment of EpCAM-overexpressing BCRs also rescued separation (Fig. 6 E). Furthermore, inhibition of PKC in wild-type tissues by pretreatment of either mesoderm explants or the BCR with bisindolylmaleimide (Bis1), a specific inhibitor of classical (α, β, γ) and novel PKC isoforms (δ, ε) phenocopied EpCAM-induced mixing (Fig. 6, F and G). We asked whether the epiboly phenotype observed upon EpCAM depletion may also be related to PKC activation: normal epiboly was fully rescued by treating EpCAM MO embryos with Bis1 (Fig. 5, G and H). Moreover, PMA treatment of wild-type embryos induced a thicker BCR (Fig. 5 I). Thus, the role of endogenous EpCAM in early development can be entirely accounted for by regulation of PKC activity.

That EpCAM negatively regulates PKC activity was directly assessed using an antibody recognizing phosphorylated PKC substrates (Fig. 7). This antibody stained multiple structures in ectoderm cells, with prominent signals at the cell periphery, at the nuclear membrane, and inside the nuclei (Fig. 7 A). EpCAM MO–injected BCRs (Fig. 7 B) showed a much more intense staining than controls, which was drastically decreased by treatment with Bis1 (not depicted) or chelerythrine chloride (another general PKC inhibitor, Fig. 7 C). The effect of EpCAM depletion on p-PKC substrates was confirmed on Western blots, with a strong increase in several major bands (not depicted).

To determine which PKC isoforms acted downstream of EpCAM, we used a panel of specific inhibitors to rescue EpCAM MO–induced epiboly defects. Because Bis1 and PMA inhibit/activate both classical (α, β, γ) and novel (δ, ε), but not atypical isoforms, we focused mainly on the first two classes. Each inhibitor was titrated, and the data from the most effective concentration (mostly about twofold above the IC50) are shown. The results clearly pointed to novel PKC isoforms because two specific inhibitors, a PKC-ε inhibitor peptide and a dominant-negative PKC-δ, both caused ectoderm–mesoderm mixing (Fig. 6 E) and rescued normal epiboly as efficiently as Bis1 or chelerythrine chloride (Fig. 5 J). Calphostin C, which has a preference for novel over classical PKCs, also fully rescued epiboly (Fig. S3). Inhibitors of classical PKC, PKC-20-28, Gö6976, and Ro-32-0432, had only weak effects, suggesting a minor contribution from the classical isoforms (Fig. 5 J and Fig. S3), and an inhibitor of atypical PKCs had no effect (Fig. 5 J).

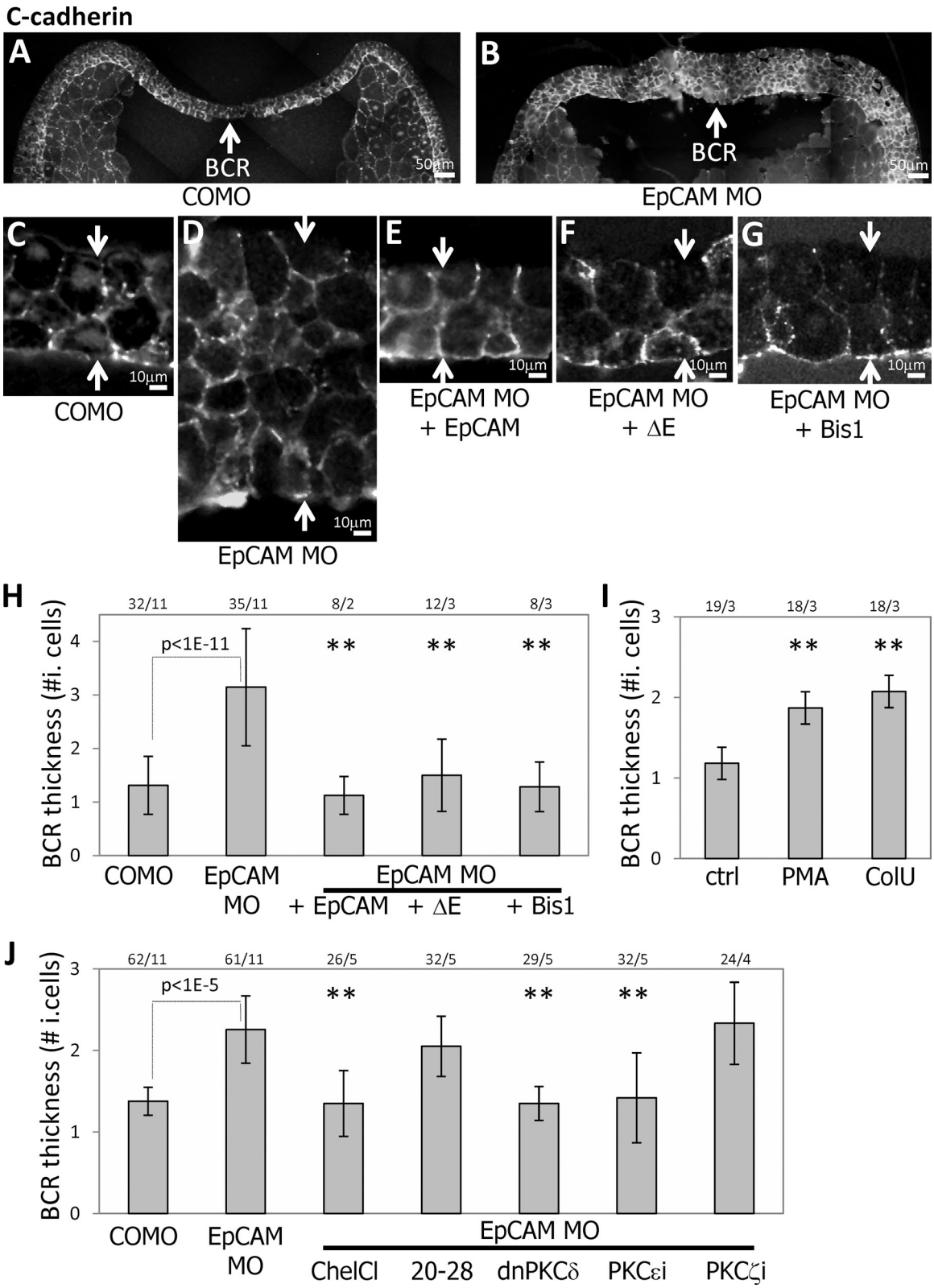

Figure 5. **Block of BCR epiboly upon EpCAM depletion and rescue by ΔE EpCAM or by PKC inhibition.** (A and B) Cross sections of early gastrula BCRs from embryos injected with control MO (COMO) and EpCAM MO. Sections were stained with anti–C-cadherin antibody. (C–F) Higher magnification views of BCRs from controls, EpCAM MO, and rescue by full-length EpCAM or ΔE mRNA coinjection. Arrows indicate the outer and inner surfaces of the BCRs. Control BCRs were 2–3 cell layers thick, including the outer layer, which does not undergo radial intercalation. EpCAM MO BCRs were much thicker. Normal morphology was rescued by EpCAM or ΔE. (G) BCR of an embryo injected with EpCAM MO and incubated for 2 h with the PKC inhibitor Bis1 before fixation. (H) Quantification of BCR thickness (counted as number of inner cell layers, excluding the outer layer). **, $P < 0.01$ compared with EpCAM MO (Student's *t* test). (I) Impaired epiboly upon treatment with PMA or Coleon U (Col U), a specific inhibitor of novel PKCs. **, $P < 0.01$ compared with controls. (J) Effect of selective PKC inhibitors on epiboly of EpCAM MO-injected embryos. **, $P < 0.01$ compared with EpCAM MO. Activator/inhibitor concentrations are listed in Materials and methods. Numbers on top indicate total number of embryos/number of experiments.

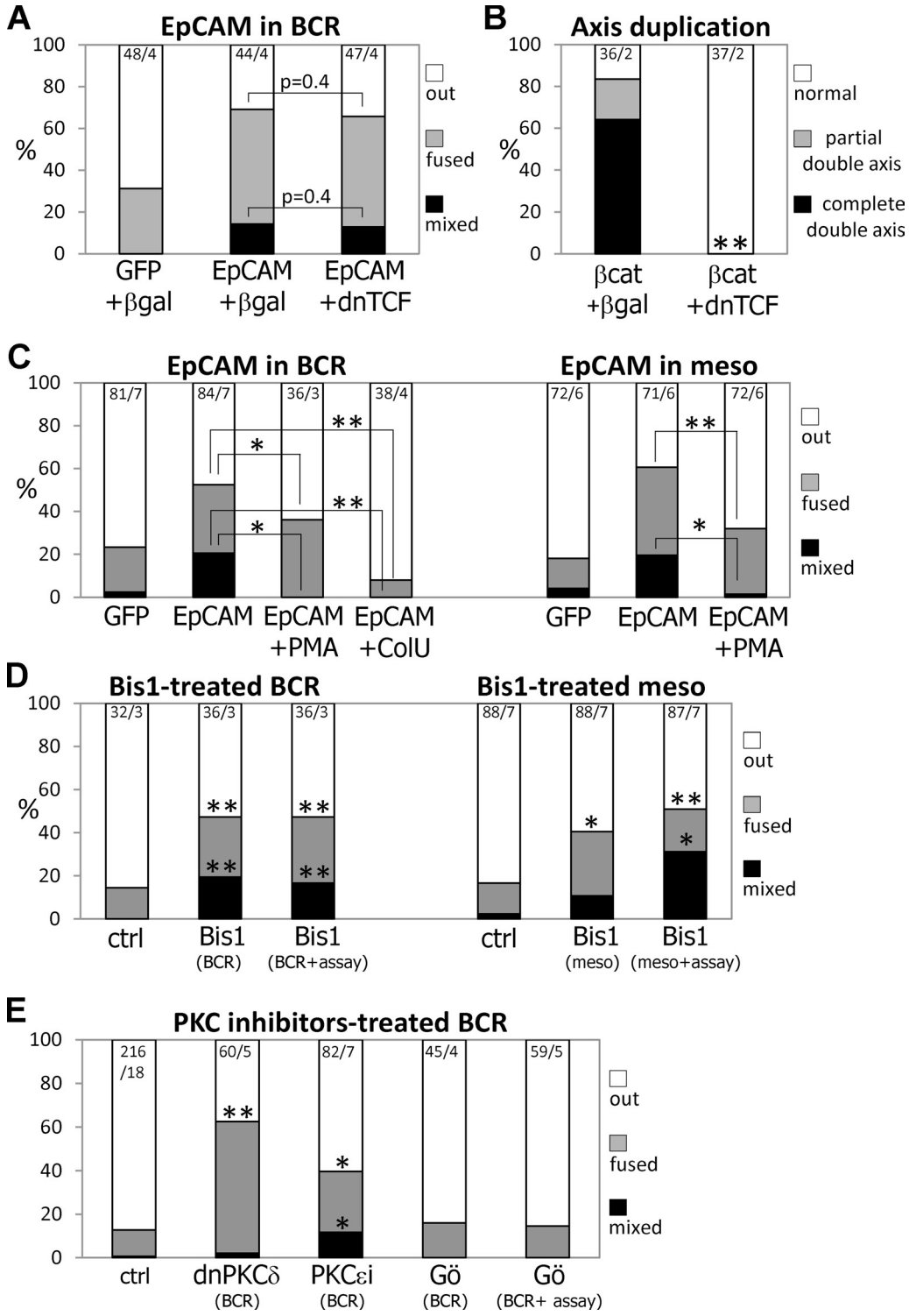

Figure 6. **EpCAM-induced tissue mixing is independent of β-cat/TCF signaling but involves down-regulation of PKC signaling.** (A) Effect of dominant-negative xTCF (dnTCF) coexpression. dnTCF does not rescue EpCAM-induced cell mixing. (B) Effect of dnTCF on secondary axis induction by β-catenin. dnTCF completely abolished double-axis induction. **, $P < 0.01$, Student's *t* test. (C) Rescue of EpCAM-induced mixing by PMA and Coleon U (ColU). EpCAM overexpressing BCRs or mesoderm explants were incubated in the presence of PMA/Coleon U for 15 min before the assay. * and **, $P < 0.05$ and $P < 0.01$, respectively, compared with EpCAM alone. (D) PKC inhibition interferes with tissue separation. Wild-type BCRs or mesoderm explants were preincubated for 15 min in the presence of 500 nM Bis1. The assay was then performed in the absence (second column) or in the presence (third column) of Bis1. * and **, $P < 0.05$ and $P < 0.01$, respectively, compared with controls. (E) Effect of PKC isoform-specific inhibitors on tissue separation. Inhibitors were added to the BCRs 15 min before assembling the assay. In the case of Gö6976, the assay was also then performed in the continuous presence of the inhibitor (last column). * and **, $P < 0.05$ and $P < 0.01$, respectively, compared with controls. Numbers on top indicate total number of explants/number of experiments.

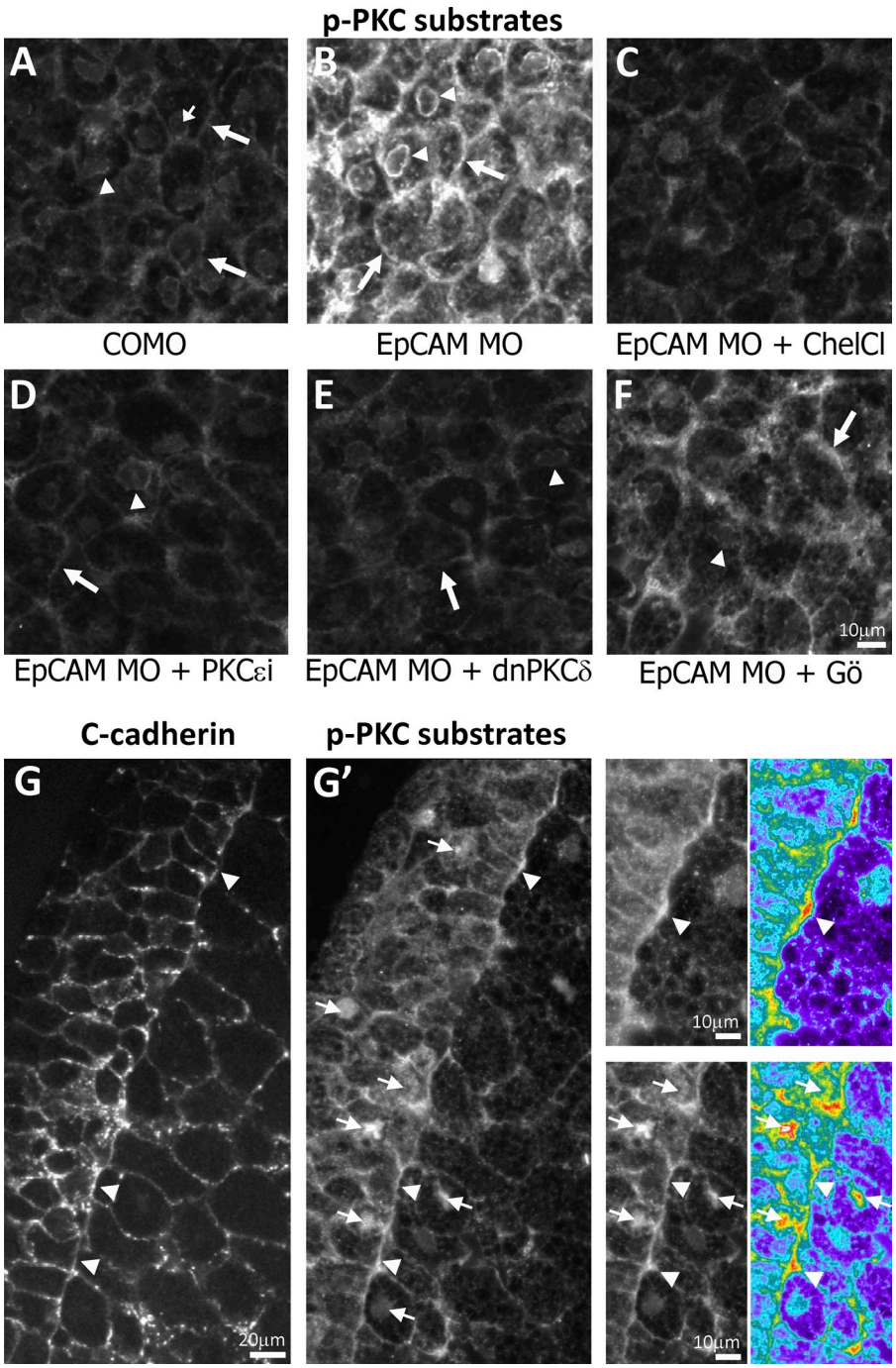

Figure 7. **PKC overactivation in EpCAM-depleted embryos, and enhanced activation at the ectoderm–mesoderm boundary.** (A–F) Cryosections of ectoderm explants stained with an antibody recognizing phosphorylated PKC substrates. (A) Control, with weak signal at the cell periphery (large arrows), in the nucleus (small arrow), and at the nuclear membrane (arrowheads). Note that not all nuclei are visible on one section. (B) Bright signal in EpCAM-depleted cells, including a prominent signal at the periphery (large arrows) and at the nuclear membrane (arrowheads). (C–E) Strong decrease after treatment of EpCAM-depleted explants with chelerythrine chloride (ChelCl, inhibitor of classical and novel PKCs), PKC-ε peptide inhibitor, or expression of dominant-negative PKC-δ. (F) Partial selective decrease (mostly cytoplasm and nuclear membrane) after treatment with Gö6976 (classical PKCs). (G and G′) Dorsal region of stage 10.5 whole-embryo section double-stained for C-cadherin (G, red channel), and phospho-PKC substrates (G′, green channel; including enlarged areas and corresponding pseudocolors). Nuclei were counterstained with Hoechst (not depicted). Exposure is higher than for panels A–F. The signal tends to be enriched along parts of Brachet's cleft (arrowheads). Other bright signals correspond mainly to nuclei and mitotic structures (small arrows).

The role of novel PKCs was further demonstrated by the fact that Coleon U, a specific activator of novel PKCs (Coutinho et al., 2009), induced BCR thickening, phenocopying EpCAM depletion (Fig. 5 J). Novel PKCs also appeared crucial for ectoderm–mesoderm separation: the PKC-ε inhibitor and the dominant-negative PKC-δ induced mixing, whereas Gö6976 had no effect (Fig. 6 F). Furthermore, Coleon U treatment of EpCAM-overexpressing BCRs fully rescued tissue separation (Fig. 6 D).

We also examined the effect of the various inhibitors on the enhanced phospho-PKC substrate staining observed in EpCAM-depleted BCRs. The signal was reduced to various degrees by inhibitors of both classical and novel PKCs (Fig. 7, C–F). Different inhibitors preferentially decreased the signal at specific subcellular locations, confirming that various PKC isoforms have distinct sets of targets. For instance, Gö6976 eliminated most of the nuclear membrane signal, but had little effect on the signal at the cell periphery. Globally, however, PKC-δ and -ε inhibitors had the strongest effect, lowering the signal close to the levels of wild-type cells. These results indicate that EpCAM depletion causes a general increase in both classical and novel PKC activities. Nevertheless, the novel isoforms seem to play a major functional role in tissue separation and epiboly. We stained sections of whole embryos, and observed a

weak but reproducible enrichment at contacts between ectoderm and mesoderm cells, scattered along the boundary (Fig. 7 G), suggesting a potential locally controlled activation.

EpCAM levels affect the actin cytoskeleton

We hypothesized that the phenotypes observed may at least partly relate to changes in the actin–myosin cytoskeleton. For instance, one may expect that increased contractility would favor a stable tissue organization and ectoderm–mesoderm separation, whereas decreased contractility would be permissive for cell movements, including tissue rearrangement such as epiboly, and cell mixing.

The influence of EpCAM levels on the actin cytoskeleton organization was examined by phalloidin staining of whole BCRs (Fig. 8, A–D), and the results confirmed by actin immunostaining on cryosections and live imaging of BCR-expressing RFP-utrophin (unpublished data): in wild-type BCRs, we observed a thin irregular staining along the cell periphery, with larger patches located at corners between three cells (Fig. 8, A and C). These patches became more prominent in EpCAM-depleted BCR, whereas the rest of the staining decreased (Fig. 8 B). The lateral punctuate pattern was restored, and the large patches at corners disappeared upon treatment with novel PKC inhibitor (Fig. 8 C), but not inhibitors of classical or atypical PKCs (unpublished data). In EpCAM-overexpressing BCRs, the patches were largely absent, and the cells became outlined by a smooth continuous staining (Fig. 8 D). Levels of phosphorylated myosin light chain detected by Western blot were reproducibly stronger in EpCAM-depleted tissues (Fig. 8 J), although only very partially rescued by dominant-negative PKC-δ.

We examined cell-protrusive activity by live confocal microscopy BCRs expressing membrane-targeted GFP (mGFP). Consistent with the pattern reported from phalloidin-stained zebrafish embryos (Slanchev et al., 2009), the basal surface of BCR cells showed wide protrusions, which were globally less and more frequent in EpCAM MO and EpCAM overexpressing BCRs, respectively (Fig. 8, E–H). A closer look at these protrusions (Fig. 8, E–H) and at their dynamics (Fig. S4, quantification presented in Fig. 8 I) revealed that EpCAM-depleted cells formed in fact many protrusions, but these were generally shorter, thinner, and most significantly short lived, as opposed to the extremely large and stable extensions produced by EpCAM-overexpressing cells.

We have recently analyzed the role of RhoA in the BCR assay and showed that blocking its activity on either side of the boundary by expression of a dominant-negative form causes mixing (unpublished data). We found here that activated RhoA could fully rescue the BCR–mesoderm boundary when co-expressed with EpCAM, either in the BCR or in the mesoderm (Fig. 8, K and L), a result consistent with a role of EpCAM in antagonizing contractility.

Discussion

Our results reveal important aspects of EpCAM biology and also provide interesting insights into the mechanisms of morphogenesis.

It had been so far difficult to reconcile the proposed role of EpCAM as an adhesion molecule (Trzpis et al., 2007) with the observed cell phenotypes, in particular its stimulatory effect on in vitro cell migration (Osta et al., 2004) and its requirement in vivo to enable cells to rearrange during epiboly (Slanchev et al., 2009). Our data provide a different view of EpCAM function in morphogenesis. Indeed, the observed loss- and gain-of-function phenotypes (epiboly phenotype, increased migration within the ectoderm, ectoderm–mesoderm mixing in both directions) can all be attributed to a single activity of EpCAM, which does not require its extracellular domain. This activity appears to impinge on a PKC-dependent pathway: (1) PKC inhibition fully rescues the loss-of-function epiboly phenotype and mimics the gain-of-function tissue mixing phenotype; (2) PKC activation interferes with epiboly and rescues the ability of an overexpressing EpCAM tissue to maintain a boundary; and (3) EpCAM levels negatively affect endogenous PKC activity. We have established that novel PKCs play a major role in tissue separation and epiboly. Together with data implicating PKC-δ in convergence extension (Kinoshita et al., 2003), novel PKCs emerge as crucial regulators of morphogenesis. We found no evidence for a role of classical, calcium-activated PKC-α/β at the cleft, at least in the most downstream events activated/inhibited during our short pretreatments. It is thus possible that PKCs are involved at two levels: classical PKCs in an upstream frizzled calcium-dependent pathway (Sheldahl et al., 1999; Medina et al., 2004), and novel PKCs in regulating more proximally the actin cytoskeleton. Note however that neither the role of classical PKC nor a direct requirement for calcium in PKC activation have been demonstrated in the context of tissue separation. Previous rescues have used PKC-α overexpression (Winklbauer et al., 2001), which may have resulted from global, nonspecific PKC overactivation. Yet, considering the many potential activities of PKCs, it is even possible that each isoform has multiple roles, of which we detect only the ones related to the most obvious phenotypes and/or to those most sensitive to modulation of PKC activity.

We show that PKC function is not restricted to the mesoderm, as previously assumed, and may in fact repress a general property of embryonic cells to move actively among other cells. Presumably, the establishment of a boundary requires this motile activity to be tamed. The widespread localization of PKC-phosphorylated substrates and the global deregulation observed in EpCAM-depleted ectoderm explants suggest that this control is in place in all cells/tissues, although the enhanced signal detected along the cleft hints at an additional local activity specifically at the boundary, an interesting possibility to be addressed in the future.

Despite EpCAM being expressed at significant levels in the mesoderm and enriched at the cleft, loss of EpCAM function did not cause obvious defects in mesoderm involution or in tissue separation (unpublished data). Whether the low levels left at this stage in MO-injected embryos are sufficient or whether EpCAM is not required in this context remains to be solved. Clearly however, a tight regulation of EpCAM levels is crucial for gastrulation: decreasing levels in the BCR lead to impaired cell mobility and block epiboly, whereas higher levels stimulate cell mobility and even cause neighboring tissues to mix.

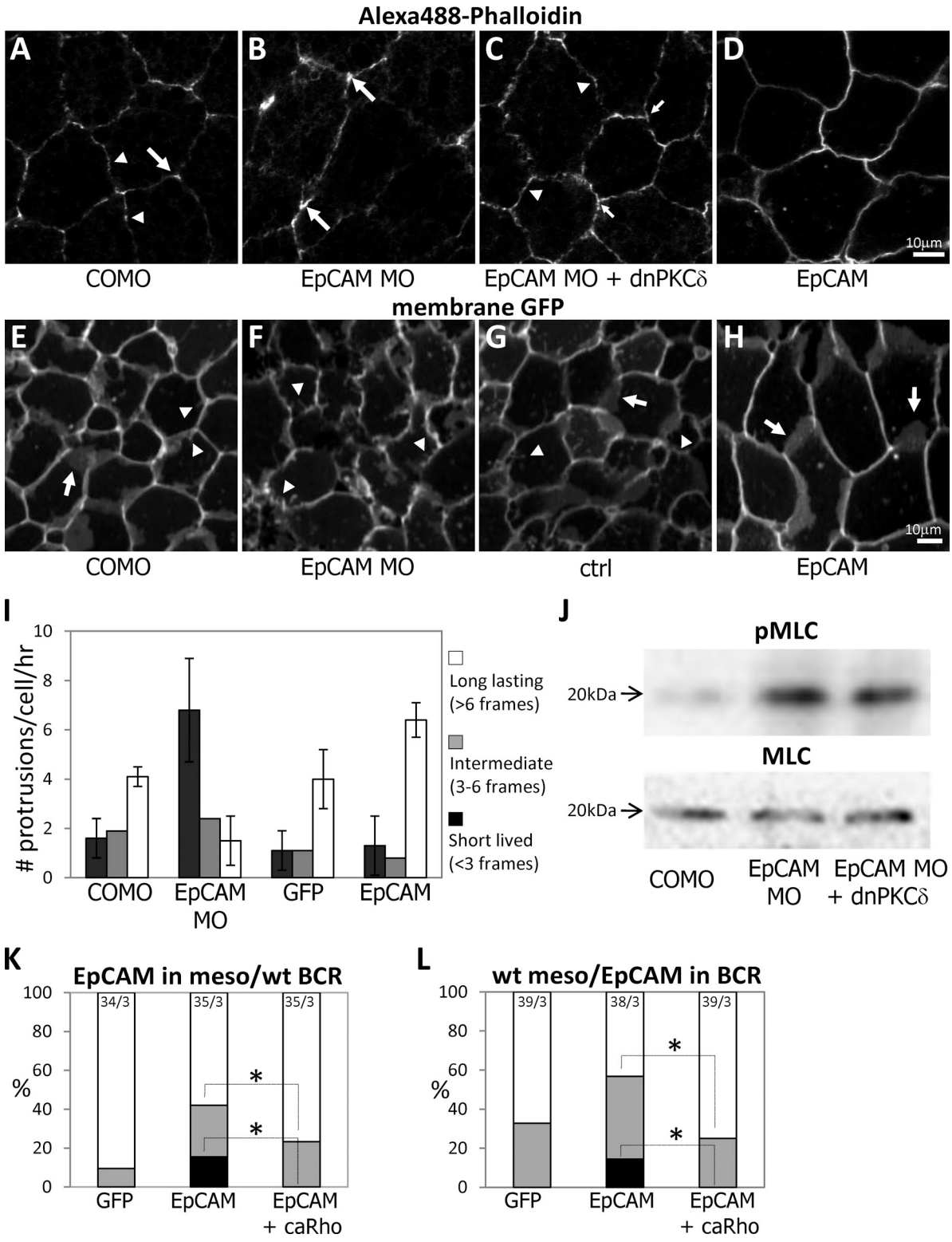

Figure 8. **Effects of EpCAM depletion on actin cytoskeleton organization, myosin phosphorylation, and protrusive activity.** (A–D) Confocal images of phalloidin-stained BCR explants. (A) Typical punctate phalloidin pattern (arrowheads) in control cells (COMO) with prominent accumulation at tricellular corners (large arrows). (B) Concentration at corners in EpCAM MO cells (large arrows), and decrease of the signal along the membranes. (C) Rescue of membrane staining and disappearance of the signal at corners upon coinjection of dominant-negative PKC-δ mRNA. (D) Homogenous membrane staining of EpCAM-overexpressing cells. (E–H) Live confocal images of the surface of membrane GFP-expressing BCR cells. Arrows: large protrusion. Arrowheads: small protrusions. (I) Quantitation of protrusive activity from time-lapse movies (see selected frames in Fig. S4). EpCAM MO-injected cells showed much fewer long-lasting protrusions than controls ($P = 2{,}5E^{-07}$; Student's *t* test) but many more short-lived extensions ($P = 5{,}4E^{-07}$). Most protrusions emanating from EpCAM-overexpressing cells were long lived ($P = 6{,}9E^{-06}$ compared with GFP controls). (J) Increased myosin light chain (MLC) phosphorylation in EpCAM MO BCRs, and partial rescue by coexpression of dominant-negative PKC-δ. (K and L) Rescue of tissue separation by coexpression of constitutively active RhoA. EpCAM mRNA (200 pg) was injected alone or with V14RhoA mRNA (25 pg). Numbers on top indicate total number of explants/number of experiments. *, $P < 0.05$ compared with EpCAM alone (Student's *t* test).

Note that EpCAM is also required for mesoderm morphogenesis at a slightly later stage (neurula), as we have observed failure of notochord cells to adopt their final arrangement in EpCAM-depleted embryos (unpublished data).

EpCAM appears to regulate cell movement via reorganization of the actin cytoskeleton, enabling cells to "flow" more freely within the tissue. Note that we still do not understand how cells "move" within these tissues. In our preliminary live images ectoderm cells seem to slide smoothly past each other (unpublished data), and we do not think that the protrusions formed along the inner surface of the ectoderm (Slanchev et al., 2009 and unpublished data) are necessarily involved in epiboly. However, these superficial structures are striking and represent a useful source of information about the dynamic state of the cytoskeleton: in the absence of EpCAM, cells appear to be frozen in a rigid, contracted state, unable to extend but very small and transient extensions. F-actin accumulates in clusters and, although we do not know their nature (the phospho-myosin signal was too weak at this stage to confirm with confidence its presence at these sites), it is tempting to speculate by analogy with other systems (Cavey et al., 2008) that they represent structures under tension involved in restricting cell rearrangements. The increased total levels of phospho-myosin in EpCAM-depleted tissues and the fact that RhoA activation rescues separation (Fig. 8) are consistent with this hypothesis. With high EpCAM levels this tight actin organization is lost and large protrusions can extend, a process classically counteracted by Rho-induced contraction. Altogether, these observations suggest an antagonism between EpCAM-dependent signaling and actin–myosin contractility.

The chemical activators and inhibitors showed effects on tissue mixing within minutes, demonstrating that this is a rather direct response to PKC modulation, even though the downstream events are likely to be complex considering the many targets of PKC. None of the other clones isolated in our screen had any obvious connection to PKC signaling (unpublished data). It should be noted, however, that the initial round of this relatively small screen (~6,000 clones) involved pools of 50–60 clones, which limited the amount of mRNA injected to 100 pg per clone. Thus, only molecules particularly active at interfering with tissue separation could be picked, a fact that emphasizes the remarkable properties of EpCAM.

Classical models of sorting at early embryonic boundaries have assumed asymmetric properties of the two apposing tissues: one of the tissues would display stronger adhesion or stronger cortical tension (Steinberg and McNutt, 1999; Krieg et al., 2008), or each tissue would express a different set of adhesion molecules (Steinberg and Takeichi, 1994). Although such differences might indeed contribute to the ectoderm–mesoderm boundary, our data show that cells from either tissue can be induced to mix in a manner that appears perfectly symmetric according to several criteria (extracellular domain not required, PKC dependence, and RhoA rescue). Furthermore, mixing occurs irrespectively of changes in cadherin surface expression in the ectoderm or in the mesoderm, indicating that the process is largely insensitive to differences in cell–cell adhesion. This surprising observation is in fact quite consistent with our previous results on the notochord–somitic boundary, where cells could sort on either side of the boundary independently of the strength of cadherin-mediated adhesion (Reintsch et al., 2005).

A physiological role for EpCAM as a bona fide cell adhesion molecule remains to be established. In our experimental model, a "compacting" phenotype consistent with such function is observed only with the highest levels of expression, and could also result from strong cadherin stabilization rather than direct EpCAM adhesion. In addition to its role in epiboly, EpCAM is required to maintain epithelial tissue integrity in zebrafish (Slanchev et al., 2009), which has been interpreted as a result of EpCAM adhesive properties. We have observed a similar requirement for EpCAM in late (post-gastrulation) *Xenopus* embryos (unpublished data). Further studies are necessary to discriminate between direct roles in adhesion, or other possible function of the extracellular domains, dependent or independent of homophilic binding (e.g., localization to membrane subdomains). EpCAM is structurally unique among CAMs. It rather resembles Notch in its general extracellular domain organization and has some distant homology with the plasminogen activator (Cirulli et al., 1998), thus molecules functioning in signaling and cell migration. In this context, EpCAM has been found to copurify with glycolipid-enriched lipid microdomains (Schmidt et al., 2004; Claas et al., 2005; Ladwein et al., 2005), which have the potential to organize signaling complexes at the cell surface.

From the available data, EpCAM rather emerges as a crucial signaling molecule, controlling two independent pathways, one regulating cell proliferation via nuclear activities, which involve β-catenin–dependent transcripton (Maetzel et al., 2009), and this novel PKC-dependent role in morphogenetic processes. The remarkable "invasive" phenotype is obviously of interest for the understanding of EpCAM function in the context of adult tissues and metastasis. It is indeed tempting to speculate that high levels of EpCAM may similarly provide cancer cells with the ability to move more actively within a tissue (and/or a tumor), help to escape the tissue of origin, and perhaps even invade other tissues.

Materials and methods

Embryo manipulations

Embryos were obtained as described previously (Danilchick et al., 1991). The culture, dissection, and injection media used are the same as in Schohl and Fagotto (2003). Embryos were injected animally at the 2-cell stage (once in each blastomere) for BCR targeting, equatorially at the 4-cell stage (once in each dorsal blastomere) for mesoderm targeting, and ventrally at the 4-cell stage (in one blastomere only) for the double-axis induction experiment. Embryonic staging was performed according to Nieuwkoop and Faber (1967). Dissections and assays were performed in MBS-H (modified barth solution containing: 88 mM NaCl, 1 mM KCl, 2.4 mM $NaHCO_3$, 0.82 mM $MgSO_4$, 0.33 mM $Ca(NO_3)_2$, 0.41 mM $CaCl_2$, 10 mM Hepes, and 10 µg/ml streptomycin sulfate and penicillin, pH 7.4 adjusted with NaOH).

Plasmids, mRNAs, and oligonucleotides

The following EpCAM cDNAs were cloned into pCS2+: EpCAM encodes full-length EpCAM (aa 1–315). EpCAM-MT corresponds to full-length EpCAM C-terminally fused to 6x myc tag, cloned into pCS2+MT. EpCAM-ΔC (aa 1–278) had the cytoplasmic tail replaced by the 6xmyc-tag of pCS2+myc. ΔE-EpCAM was constructed by fusing the signal sequence and the fifth extracellular repeat of C-cadherin (gift from P. Hausen,

Max-Planck-Institut für Entwicklungsbiologie, Tuebingen, Germany) to a fragment of EpCAM lacking most of its extracellular domain (aa 265–315), cloned into pCS2+MT, containing a C-terminal 6x myc-tag; ΔEΔ247 and ΔEΔ253 (deletion of the cytoplasmic tail after aa 247 and aa 253) and ΔE-EpCAM-NQ (point mutations K243N and K244Q) and ΔE-QQ (R242Q and K244Q) were generated from ΔE-EpCAM by site-directed mutagenesis. Other plasmids used: dnXTCF in pT7Ts (Molenaar et al., 1996), Myc-eGFP (Reintsch et al., 2005) and β-galactosidase in pCS2+ (Rupp et al., 1994), dominant-negative PKC-δ (Kinoshita et al., 2003), and membrane-targeted GAP43-eGFP.

All pCS-EpCAM plasmids were linearized with NotI and mRNAs were synthesized in vitro using SP6 RNA polymerase.

Morpholino oligonucleotides: Control MO, 5′-CCTCTTACCTCAGTTACAATTTATA-3′ (human β-globin mutant sequence); EpCAM1 MO, 5′-CTTCATCCTCCAACAGACGGAACCC-3′. EpCAM2 MO, 5′-GCCTCAGAGCTGTAACGAGCTGCAT-3′; injected doses were 2 × 40 ng control MO or 2 x 20 ng EpCAM MO1 + 20 ng EpCAM MO2 per embryo.

Antibodies

Antibodies used in this study were rabbit anti-EpCAM antibody (raised against the cytoplasmic tail of EpCAM fused to GST), mouse anti–C-cadherin mAb 5G5 and rabbit anti–C-cadherin (generous gifts of B.M. Gumbiner, University of Virginia, Charlottesville, VA), mouse anti-myc tag mAb 9E10, mouse anti–β-catenin mAb H102 (Santa Cruz Biotechnology, Inc.), mouse anti–α-actinin antibody and rabbit anti-actin (Abcam) rabbit anti–phosphomyosin light chain and anti–phospho-PKC substrates (Cell Signaling Technology), and mouse anti-GFP mAb 3E6 (Invitrogen).

PKC agonists and antagonists

Concentrations used and suppliers: phorbol-12-myristate-13-acetate (PMA), 32 nM; bisindolylmaleimide I (Bis1), 500 nM; calphostin C, chelerythrine chloride (ChelCl), 1 µM; Gö6976, 20 nM; PKC-20-28, 20 µM; Ro-32-0432, 30 nM; all from EMD. PKC-ε inhibitor peptide, 5 µg/ml, Santa Cruz Biotechnology, Inc.. PKC-ζ peptide inhibitor, 2.5 µM, Enzo Life Sciences, Inc. Coleon U was a generous gift from Dr. M.F. Simões (University of Lisbon, Lisbon, Portugal). It was used at 5 µM for epiboly and 10 µM for mixing assays. They were all prepared from >400x stock solutions in DMSO.

Explants

Tissue separation assays. The tissue separation assays were performed largely as described in Wacker et al. (2000). One modification from the original protocol was the source of mesoderm. To ensure that the exact same region of the mesoderm would be dissected, independent of potential effects of exogenously expressed proteins on involution, we used, rather than involuted mesoderm, earlier preinvoluted mesoderm dissected from stage 10+ embryos (Winklbauer et al., 2001). Non-involuted mesoderm already displays strong separation behavior in the assay (Wacker et al., 2000). Statistical significance was determined using the Student's *t* test, each experiment (2–3 BCRs and 8–15 explants) being treated as the experimental unit.

Sandwich assays and inner cell explants. Embryos were injected animally at the 2-cell stage. BCRs and mesoderm pieces were dissected from stage 10+ embryos. Sandwiches were gently pressed with a coverslip and cultured for 2 h in 1x MBS-H, then fixed in 4% paraformaldehyde, embedded in 2% low-melting agarose, permeabilized in 1x PBS + 1% Triton X-100, infiltrated with fish gelatin, and processed for cryosectioning and immunostaining as described previously (Fagotto and Brown, 2008). Explants of inner ectodermal cells were prepared from stage 10 BCRs by peeling off the inner cell layer using an eyelash. The explants were placed in 1x MBS-H in 1% agarose-coated dishes and cultured for 2 h before fixation, agarose embedding, cryosectioning, and immunostaining.

Cell migration in sandwich assays were repeated in three independent experiments. The percentage of cells in each category was calculated for each explant, and averaged for each experiment. The values were calculated as average of the three experiments (the average from all explants combined gave virtually identical values). Statistical significance was determined using the Student's *t* test, using each sandwich as the experimental unit.

Immunofluorescence

Cryosectioning and immunofluorescence were performed as described previously (Schohl and Fagotto, 2002; Fagotto and Brown, 2008). Images were obtained using either an epifluorescence microscope (Axiovert TV135; Carl Zeiss, Inc.) equipped with a 25x N.A. 0.8 water immersion objective (Carl Zeiss, Inc.) and a CCD camera (Retiga 2000R; Quantitative Imaging Corporation), or an epifluorescence microscope (DM IRE2; Leica) equipped with a 20x/0.70 IMM Corr CS oil immersion objective and an ORCA-ER camera (Hamamatsu Photonics). Images were acquired using AnalySIS (Soft Imaging System GmbH) and MetaMorph (MDS Analytical Technologies) software. Large fields were reconstituted by collating pictures of adjacent regions (Schohl and Fagotto, 2002). Images of explants were acquired using a stereomicroscope (model MZ16F; Leica), a QImaging camera (MicroPublisher 3.3 RTV) and QCapture image acquisition software (Quantitative Imaging Corporation).

Quantification of rectilinearity of reconstituted boundaries

Images of the interface between BCR and mesoderm explants were divided in segments of ∼8-cell diameter. For each segment, the length of the interface, measured using the R software (http://www.r-project.org), was divided by the length of the straight line connecting its ends. This ratio provided a measurement for straightness of the boundary. Data collected from three independent experiments, with a total of 11–12 sandwiches per condition, were analyzed using ANOVA.

Phalloidin staining

Dissected BCRs were put inner layer facing down on the glass of a FluoroDish chamber (World Precision Instruments), then covered with a small piece of a Minicell-CM 0.4-µm membrane and a piece of coverglass secured with silicone grease and flattened by gently pressing the coverglass down. The membrane was inserted to improve diffusion during staining. BCRs were fixed in 4% formaldehyde in MBSX for 10 min, followed by 5 min permeabilization in 1% formaldehyde, 0.1% Triton X-100, 1 h incubation with blocking buffer (10% sheep serum), and overnight incubation with 2U/ml Alexa 488–phalloidin (Invitrogen) in 10% sheep serum. Images from planes ∼3–5 µm inside the inner BCR surface were taken with a laser scanning microscope (LSM 510; Carl Zeiss, Inc.) with a 40x Neofluar NA 1.3 oil objective.

Fluorescence live imaging

All experiments were performed at room temperature. Dissected BCRs were flattened on glass coated for 30 min with 1 µg/ml fibronectin (Sigma-Aldrich) and blocked for 10 min with 1% bovine serum albumin. The inner BCR surface was imaged with a WaveFX spinning disc confocal (Quorum Technologies) mounted on an automated microscope (model DMI6000B; Leica), with a 20x HC Plan-Apochromat CS, NA 0.7 oil objective. Images were collected every 6 min with an EM CCD camera (512 x 512 BT; Hamamatsu Photonics) and controlled with Volocity 3DM software (PerkinElmer). For each condition, 5–6 cells were picked randomly in each image (4–5 images, from different BCRs, per condition, repeated in three independent experiments, with a total of 70 cells per condition), and protrusions were followed over 10 frames to determine their life span. Statistical significance was determined using the Student's *t* test.

Online supplemental material

Fig. S1 presents the amino acid sequences of *Xenopus laevis* EpCAMa and b pseudoalleles aligned with EpCAMs of representative vertebrate species. Fig. S2 A shows a diagram of the EpCAM constructs used in this study. Fig. S2, B and C, show that the C-terminally myc-tagged EpCAM has the same tissue-mixing activity as wild-type EpCAM (B), and that the mixing activity resides in specific residues of the cytoplasmic tail proximal to the transmembrane domain (C). Fig. S3 shows epiboly rescue experiments by various PKC inhibitors. Fig. S4 presents selected frames from live time-lapse movies illustrating the effect of EpCAM level protrusion dynamics. Online supplemental material is available at http://www.jcb.org/cgi/content/full/jcb.201004074/DC1.

We thank Dr. Patrick Lemaire for the generous gift of the cDNA library, Dr. Barry Gumbiner for antibodies, Dr. Fátima Simões for Coleon U, and Dr. Noriyuki Kinoshita for the dnPKC-δ construct. We thank Caolan Kovach-Orr for writing codes and help with statistical analysis. We thank members of the laboratory and Dr. Rudi Winklbauer for critical reading of the manuscript.

This work was supported by CCSRI grant 017162 to F. Fagotto. N. Maghzal is recipient of a Canderell McGill Cancer Centre award and a HydroQuebec fellowship.

Submitted: 14 April 2010
Accepted: 4 October 2010

References

Balzar, M., H.A.M. Bakker, I.H. Briaire-de-Bruijn, G.J. Fleuren, S.O. Warnaar, and S.V. Litvinov. 1998. Cytoplasmic tail regulates the intercellular adhesion function of the epithelial cell adhesion molecule. *Mol. Cell. Biol.* 18:4833–4843.

Cavey, M., M. Rauzi, P.F. Lenne, and T. Lecuit. 2008. A two-tiered mechanism for stabilization and immobilization of E-cadherin. *Nature.* 453:751–756. doi:10.1038/nature06953

Chung, H.A., T.S. Yamamoto, and N. Ueno. 2007. ANR5, an FGF target gene product, regulates gastrulation in *Xenopus*. *Curr. Biol.* 17:932–939. doi:10.1016/j.cub.2007.04.034

Cirulli, V., L. Crisa, G.M. Beattie, M.I. Mally, A.D. Lopez, A. Fannon, A. Ptasznik, L. Inverardi, C. Ricordi, T. Deerinck, et al. 1998. KSA antigen Ep-CAM mediates cell-cell adhesion of pancreatic epithelial cells: morphoregulatory roles in pancreatic islet development. *J. Cell Biol.* 140:1519–1534. doi:10.1083/jcb.140.6.1519

Claas, C., J. Wahl, D.J. Orlicky, H. Karaduman, M. Schnölzer, T. Kempf, and M. Zöller. 2005. The tetraspanin D6.1A and its molecular partners on rat carcinoma cells. *Biochem. J.* 389:99–110. doi:10.1042/BJ20041287

Coutinho, I., G. Pereira, M.F. Simões, M. Côrte-Real, J. Gonçalves, and L. Saraiva. 2009. Selective activation of protein kinase C-delta and -epsilon by 6,11,12,14-tetrahydroxy-abieta-5,8,11,13-tetraene-7-one (coleon U). *Biochem. Pharmacol.* 78:449–459. doi:10.1016/j.bcp.2009.04.026

Danilchick, M., H.B. Peng, and B.K. Kay. 1991. *Xenopus laevis*: Practical uses in cell and molecular biology. Pictorial collage of embryonic stages. *Methods Cell Biol.* 36:679–681. doi:10.1016/S0091-679X(08)60305-2

de Boer, C.J., J.H. van Krieken, C.M. Janssen-van Rhijn, and S.V. Litvinov. 1999. Expression of Ep-CAM in normal, regenerating, metaplastic, and neoplastic liver. *J. Pathol.* 188:201–206. doi:10.1002/(SICI)1096-9896(199906)188:2<201::AID-PATH339>3.0.CO;2-8

Fagotto, F., and C.M. Brown. 2008. Detection of nuclear β-catenin in *Xenopus* embryos. *Methods Mol. Biol.* 469:363–380. doi:10.1007/978-1-60327-469-2_23

Fagotto, F., K. Guger, and B.M. Gumbiner. 1997. Induction of the primary dorsalizing center in *Xenopus* by the Wnt/GSK/beta-catenin signaling pathway, but not by Vg1, Activin or Noggin. *Development.* 124:453–460.

Hukriede, N.A., T.E. Tsang, R. Habas, P.L. Khoo, K. Steiner, D.L. Weeks, P.P. Tam, and I.B. Dawid. 2003. Conserved requirement of Lim1 function for cell movements during gastrulation. *Dev. Cell.* 4:83–94. doi:10.1016/S1534-5807(02)00398-2

Keller, R.E. 1980. The cellular basis of epiboly: an SEM study of deep-cell rearrangement during gastrulation in *Xenopus laevis*. *J. Embryol. Exp. Morphol.* 60:201–234.

Kinoshita, N., H. Iioka, A. Miyakoshi, and N. Ueno. 2003. PKC δ is essential for Dishevelled function in a noncanonical Wnt pathway that regulates *Xenopus* convergent extension movements. *Genes Dev.* 17:1663–1676. doi:10.1101/gad.1101303

Koprowski, H., Z. Steplewski, K. Mitchell, M. Herlyn, D. Herlyn, and P. Fuhrer. 1979. Colorectal carcinoma antigens detected by hybridoma antibodies. *Somatic Cell Genet.* 5:957–971. doi:10.1007/BF01542654

Krieg, M., Y. Arboleda-Estudillo, P.H. Puech, J. Käfer, F. Graner, D.J. Müller, and C.P. Heisenberg. 2008. Tensile forces govern germ-layer organization in zebrafish. *Nat. Cell Biol.* 10:429–436. doi:10.1038/ncb1705

Ladwein, M., U.F. Pape, D.S. Schmidt, M. Schnölzer, S. Fiedler, L. Langbein, W.W. Franke, G. Moldenhauer, and M. Zöller. 2005. The cell-cell adhesion molecule EpCAM interacts directly with the tight junction protein claudin-7. *Exp. Cell Res.* 309:345–357. doi:10.1016/j.yexcr.2005.06.013

Litvinov, S.V., H.A. Bakker, M.M. Gourevitch, M.P. Velders, and S.O. Warnaar. 1994. Evidence for a role of the epithelial glycoprotein 40 (Ep-CAM) in epithelial cell-cell adhesion. *Cell Adhes. Commun.* 2:417–428. doi:10.3109/15419069409004452

Litvinov, S.V., M. Balzar, M.J. Winter, H.A.M. Bakker, I.H. Briaire-de Bruijn, F. Prins, G.J. Fleuren, and S.O. Warnaar. 1997. Epithelial cell adhesion molecule (Ep-CAM) modulates cell-cell interactions mediated by classic cadherins. *J. Cell Biol.* 139:1337–1348. doi:10.1083/jcb.139.5.1337

Maetzel, D., S. Denzel, B. Mack, M. Canis, P. Went, M. Benk, C. Kieu, P. Papior, P.A. Baeuerle, M. Munz, and O. Gires. 2009. Nuclear signalling by tumour-associated antigen EpCAM. *Nat. Cell Biol.* 11:162–171. doi:10.1038/ncb1824

Medina, A., R.K. Swain, K.-M. Kuerner, and H. Steinbeisser. 2004. *Xenopus* paraxial protocadherin has signaling functions and is involved in tissue separation. *EMBO J.* 23:3249–3258. doi:10.1038/sj.emboj.7600329

Molenaar, M., M. van de Wetering, M. Oosterwegel, J. Peterson-Maduro, S. Godsave, V. Korinek, J. Roose, O. Destrée, and H. Clevers. 1996. XTcf-3 transcription factor mediates beta-catenin-induced axis formation in *Xenopus* embryos. *Cell.* 86:391–399. doi:10.1016/S0092-8674(00)80112-9

Münz, M., C. Kieu, B. Mack, B. Schmitt, R. Zeidler, and O. Gires. 2004. The carcinoma-associated antigen EpCAM upregulates c-myc and induces cell proliferation. *Oncogene.* 23:5748–5758. doi:10.1038/sj.onc.1207610

Nieuwkoop, P.D., and J. Faber. 1967. Normal table of *Xenopus laevis* (Daudin). A systematical and chronological survey of the development from the fertilized egg till the end of metamorphosis. North-Holland Pub. Co., Amsterdam.

Osta, W.A., Y. Chen, K. Mikhitarian, M. Mitas, M. Salem, Y.A. Hannun, D.J. Cole, and W.E. Gillanders. 2004. EpCAM is overexpressed in breast cancer and is a potential target for breast cancer gene therapy. *Cancer Res.* 64:5818–5824. doi:10.1158/0008-5472.CAN-04-0754

Reintsch, W.E., A. Habring-Mueller, R.W. Wang, A. Schohl, and F. Fagotto. 2005. β-Catenin controls cell sorting at the notochord-somite boundary independently of cadherin-mediated adhesion. *J. Cell Biol.* 170:675–686. doi:10.1083/jcb.200503009

Rupp, R.A., L. Snider, and H. Weintraub. 1994. *Xenopus* embryos regulate the nuclear localization of XMyoD. *Genes Dev.* 8:1311–1323. doi:10.1101/gad.8.11.1311

Schmidt, D.S., P. Klingbeil, M. Schnölzer, and M. Zöller. 2004. CD44 variant isoforms associate with tetraspanins and EpCAM. *Exp. Cell Res.* 297:329–347. doi:10.1016/j.yexcr.2004.02.023

Schohl, A., and F. Fagotto. 2002. β-catenin, MAPK and Smad signaling during early *Xenopus* development. *Development.* 129:37–52.

Schohl, A., and F. Fagotto. 2003. A role for maternal beta-catenin in early mesoderm induction in *Xenopus. EMBO J.* 22:3303–3313. doi:10.1093/emboj/cdg328

Sheldahl, L.C., M. Park, C.C. Malbon, and R.T. Moon. 1999. Protein kinase C is differentially stimulated by Wnt and Frizzled homologs in a G-protein-dependent manner. *Curr. Biol.* 9:695–698. doi:10.1016/S0960-9822(99)80310-8

Slanchev, K., T.J. Carney, M.P. Stemmler, B. Koschorz, A. Amsterdam, H. Schwarz, and M. Hammerschmidt. 2009. The epithelial cell adhesion molecule EpCAM is required for epithelial morphogenesis and integrity during zebrafish epiboly and skin development. *PLoS Genet.* 5:e1000563. doi:10.1371/journal.pgen.1000563

Steinberg, M.S., and P.M. McNutt. 1999. Cadherins and their connections: adhesion junctions have broader functions. *Curr. Opin. Cell Biol.* 11:554–560. doi:10.1016/S0955-0674(99)00027-7

Steinberg, M.S., and M. Takeichi. 1994. Experimental specification of cell sorting, tissue spreading, and specific spatial patterning by quantitative differences in cadherin expression. *Proc. Natl. Acad. Sci. USA.* 91:206–209. doi:10.1073/pnas.91.1.206

Trzpis, M., P.M. McLaughlin, L.M. de Leij, and M.C. Harmsen. 2007. Epithelial cell adhesion molecule: more than a carcinoma marker and adhesion molecule. *Am. J. Pathol.* 171:386–395. doi:10.2353/ajpath.2007.070152

Wacker, S., K. Grimm, T. Joos, and R. Winklbauer. 2000. Development and control of tissue separation at gastrulation in *Xenopus. Dev. Biol.* 224:428–439. doi:10.1006/dbio.2000.9794

Winklbauer, R., and R.E. Keller. 1996. Fibronectin, mesoderm migration, and gastrulation in *Xenopus*. *Dev. Biol.* 177:413–426. doi:10.1006/dbio.1996.0174

Winklbauer, R., A. Medina, R.K. Swain, and H. Steinbeisser. 2001. Frizzled-7 signalling controls tissue separation during *Xenopus* gastrulation. *Nature.* 413:856–860. doi:10.1038/35101621

Zeng, L., F. Fagotto, T. Zhang, W. Hsu, T.J. Vasicek, W.L. Perry III, J.J. Lee, S.M. Tilghman, B.M. Gumbiner, and F. Costantini. 1997. The mouse Fused locus encodes Axin, an inhibitor of the Wnt signaling pathway that regulates embryonic axis formation. *Cell.* 90:181–192. doi:10.1016/S0092-8674(00)80324-4